

# Stability of Jordan Recurrent Neural Network Estimator

Avneet Kaur\*, Ruikun Zhou\*, Jun Liu and Kirsten Morris

**Abstract**—State estimation involves finding the states of a noisy dynamical system with a noisy initial condition using noisy measurements, given a model of the system. Many methods exist for state estimation of dynamical systems. For linear dynamical systems with white Gaussian noises of known mean and variance, Kalman filtering is an optimal state estimation algorithm. While several extensions of the Kalman filter to nonlinear systems exist, either the method is not optimal or calculation is not feasible. Several approaches using neural networks have been developed in recent years. While these approaches seem to work numerically, stability and convergence guarantees do not exist. In this paper, we propose to use a Jordan recurrent neural network (JRN) for state estimation. An input-to-state stability (ISS) analysis of the error dynamics is used. Our results are compared to the Kalman filter for the linear case and the extended Kalman filter for the nonlinear case.

## I. INTRODUCTION

State estimation refers to estimating the states of a noisy dynamical system given noisy and incomplete measurements, partial information about the initial state, as well as a mathematical model for the system. In practical applications, estimating the state of a system is a challenging task for various reasons. The complexity of high-order systems, the availability of a finite number of measurements, inaccurate measurements, incomplete information about the initial state, and errors in the model can make it difficult to estimate the state of the system.

One of the most commonly used optimal state estimation methods is the Kalman filter (KF) [1]. It is optimal for linear systems with white Gaussian noises with zero mean and known covariance. When implemented for a discrete-time system, it consists of two steps: prediction and filtering, and is a recursive algorithm. Many researchers have extended the Kalman filter to nonlinear systems. The most obvious model-based generalization of this filter to nonlinear systems is the Extended Kalman filter (EKF) [2] [3]. The EKF relies on linearization of the dynamical system at each time-step. Although local convergence guarantees [4], [5] exist, convergence to the true state is an issue for highly nonlinear systems and when the estimate of the initial condition is very inaccurate. Moreover, even when the estimation error converges to zero, the method is not optimal.

\* Both authors contributed equally to this work.

This work was supported by the University of Waterloo and NSERC (Canada).

Avneet Kaur, Ruikun Zhou, Jun Liu and Kirsten Morris are with the Faculty of Mathematics, Department of Applied Mathematics, University of Waterloo, 200 University Ave W, Waterloo, Canada a93kaur@uwaterloo.ca, ruikun.zhou@uwaterloo.ca, j.liu@uwaterloo.ca, kmorris@uwaterloo.ca.

In recent years, machine learning approaches, particularly artificial neural networks, have attracted attention. Gao *et al.* [6] used deep long short-term memory (DLSTM) networks to approximate the predicted and filtered state from observations. Although they aimed to study trajectory tracking, their approach turned out to be a state estimation problem since they ignored certain assumptions and used knowledge of the model for training dataset generation. They presented two frameworks, Bayesian and non-Bayesian. For the Bayesian approach, they used Bayes' rule [7] and designed the DLSTM so that it predicts and filters iteratively within the same network. For the non-Bayesian approach, they considered two DLSTM networks, one for prediction and the other for filtering, based on the fact that neural networks can perform both steps independently. Thus, one network performed prediction without measurements, and the other corrected the predictions by using new measurements. Estimation accuracy, error bounds, analytic performance evaluation, and neural network convergence remain open problems for these approaches. Breitan *et al.* [8] proposed a machine learning framework that overcame the requirement to find solutions to the Hamilton-Jacobi-Bellman (HJB) partial differential equation for an optimal estimator in the continuous-time case. A neural network was used to approximate the gradient of the solution of the HJB equation. They exploited the HJB equation to construct the observer gain, which coincided with the Kalman-Bucy filter for a linear system. Peralez [9] further proposed a deep learning-based Luenberger estimator design for discrete-time nonlinear systems by approximating the mapping using unsupervised learning. Gençay *et al.* [10] compared the method of least squares, Elman recurrent neural network (ERN), and feedforward neural networks (FNN) for noisy time series data with fully observable states. They concluded that ERNs provided the best estimation properties among the three.

Identifying states entirely on the basis of input-output data is called system identification. Recurrent neural networks have been shown to work well for system identification [11]. In fact, Jordan recurrent networks (JRN) have been used for system identification by several researchers and have been shown to work as well as ERNs [12][13]. A convergence analysis, with some assumptions, of both networks for system identification has been discussed in [14]. Forecasting is a domain in which future values are predicted based on observed trends. In [15], an Elman-based long short-term memory (LSTM) network is compared with an EKF for time series forecasting. The authors conclude that the LSTM performs better than the EKF for nonlinear systems. In [16], authors show that the ERN performs at least as well as FNN

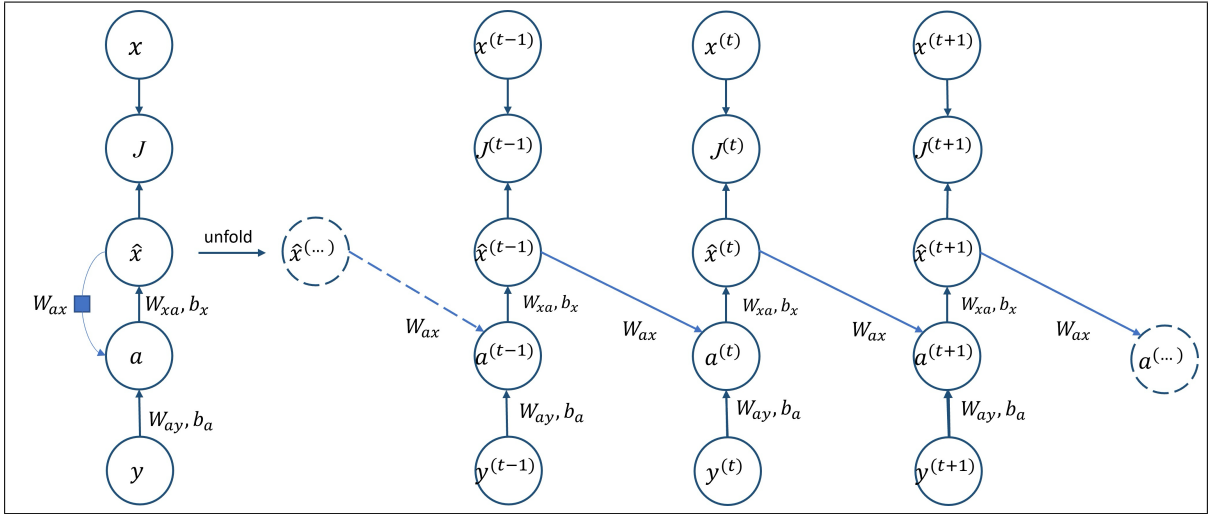


Fig. 1: The structure of the Jordan recurrent network proposed for state estimation. It uses output-to-hidden recurrent connections similar to the filter’s dynamical system. The symbols  $y^{(t)}$ ,  $a^{(t)}$ ,  $x^{(t)}$  and  $\hat{x}^{(t)}$  represent input measurement vector, hidden layer vector, true state vector and estimated state vector respectively at time  $t$ . Cost function  $J^{(t)}$  is the mean squared error at time  $t$ . The weights and biases of the network are represented by  $W_{ay}$ ,  $W_{ax}$ ,  $W_{xa}$ ,  $b_x$  and  $b_y$ .

for Lyapunov exponents forecasting, discussing cases where it performs better in detail as well.

This encouraged us to use recurrent neural networks for state estimation. The issue with ERNs is that proving the stability of the estimator is difficult, as the dependence is not directly on the estimated state but on the hidden state at the previous time-step. This is not the case for a JRN. We use an algorithm that uses known information about a dynamical system to train a JRN for state estimation. The structure of JRN resembles that of a dynamical system, making it a suitable candidate for state estimation. The difference between Elman and Jordan recurrent neural networks lies in the types of recurrent connections [17]. Schäfer and Zimmerman [18] proved ERNs are universal approximators of dynamical systems. These results can be extended to JRN for state estimation [19].

The stability of recurrent neural networks (RNNs) in the sense of Lyapunov has been well-developed in [20], [21], although the stability of errors in RNNs as neural estimators for state estimation has not been extensively explored. Finding Lyapunov functions is generally challenging. Several papers [22], [23] have shown that Lyapunov functions can be attained and represented by expressions of the compositional structure of the neural network, the correctness being guaranteed by satisfiability modulo theories (SMT) solvers. In this paper, we design an estimator using JRN and employ an input-to-state stability (ISS) approach to analyze the stability of the error dynamics. We provide a theoretical result establishing a condition under which the error dynamics will converge to zero if the original system is stable. Estimation of unstable systems is generally conducted in combination with a stabilizing feedback, so our approach assumes that any necessary stabilization has been performed. The corresponding Lyapunov functions are

learned by FNNs using an ISS approach. To the best of the authors’ knowledge, this is the first work analyzing the stability of errors using ISS and finding the ISS Lyapunov function with a neural network for state estimation.

We use a hybrid approach that combines both model and data. We employ a shallow JRN, presented in Section II and Section III-A, to estimate the states of the dynamical system. Data for training the recurrent network is model-based and generated as explained in Section II-B. This ensures that the training data reflect the assumptions of a Kalman filter and an extended Kalman filter. Input-to-state stability analysis of the Jordan recurrent network-based estimator is discussed in Section II, while the method to find the corresponding Lyapunov functions is explained in Section II-B. The approach is then tested in Section IV on three different discrete-time systems, obtained from the discretization of ODEs, one linear and two nonlinear. This is followed by a discussion of the convergence and input-to-state stability of the results.

## II. INPUT-TO-STATE STABILITY ANALYSIS

Consider a discrete-time nonlinear system

$$\begin{aligned} x^{(t+1)} &= f(x^{(t)}) + w^{(t+1)}, \\ y^{(t+1)} &= h(x^{(t+1)}) + v^{(t+1)}, \\ x^{(0)} &= x^0 + \bar{x}^0, \end{aligned} \quad (1)$$

where  $x^{(t)} \in \mathcal{X} \subseteq \mathbb{R}^n$  is the state vector at time-step  $t$ ,  $w^{(t+1)} \in \mathbb{R}^n$  is the process noise vector at time-step  $t + 1$ ,  $y^{(t+1)} \in \mathcal{Y} \subseteq \mathbb{R}^m$  is the measurement vector at time-step  $t + 1$ ,  $v^{(t+1)} \in \mathbb{R}^m$  is the measurement noise vector at time-step  $t + 1$ ,  $x^0 \in \mathbb{R}^n$  is the true initial condition and  $\bar{x}^0 \in \mathbb{R}^n$  is the initial condition noise. Here,  $\mathcal{X}$  and  $\mathcal{Y}$  are the state space and measurement space, respectively, and  $n \in \mathbb{N}$  is the total number of states and  $m \in \mathbb{N}$  is the number of states

whose noisy measurements are available. The functions  $f$  and  $h$  are assumed to be sufficiently smooth.

Our aim is to estimate the state vector  $x^{(t+1)}$  by  $\hat{x}^{(t+1)}$  based on the measurement vector  $y^{(t+1)}$ , previous state vector estimate  $\hat{x}^{(t)}$  and the unknown noisy initial condition  $x^{(0)}$ .

A JRN has recurrent connections from the output of the previous layer to the hidden state of the next layer. Thus, we use  $y^{(t+1)}$  and  $\hat{x}^{(t+1)}$  as inputs and outputs, respectively, of the JRN. The forward propagation of the network is

$$\begin{aligned} a^{(t+1)} &= \sigma(W_{ay}y^{(t+1)} + W_{ax}\hat{x}^{(t)}), \\ \hat{x}^{(t+1)} &= W_{xa}a^{(t+1)}, \end{aligned} \quad (2)$$

where  $\sigma$  is the activation function and  $\hat{x}^{(t+1)}$  is the estimated state vector at time-step  $t+1$ . The hidden layer vector at time-step  $t+1$  is given by  $a^{(t+1)}$ . The weights and biases of the network are represented by  $W_{ay}$ ,  $W_{ax}$  and  $W_{xa}$ . The network is depicted in Fig. 1. This is different from an ERN because the recurrent connections for an ERN are from the previous hidden layer  $a^{(t)}$  to the next hidden layer  $a^{(t+1)}$ , whereas for a JRN, they are from the previous output  $\hat{x}^{(t)}$  to next hidden layer  $a^{(t+1)}$ . Thus, for an ERN, the term  $W_{ax}\hat{x}^{(t)}$  would be replaced by  $W_{aa}a^{(t)}$  where  $W_{aa}$  is a weight matrix. Note that we are considering a bias-free network.

To analyze the stability of the neural estimator, we first consider the case where there are no process noise and measurement noise in (1), i.e.,  $w^{(t+1)} = v^{(t+1)} = 0$  for all  $t$ , and  $\bar{x}^0 = 0$ , as follows,

$$\begin{aligned} x^{(t+1)} &= f(x^{(t)}), \\ y^{(t+1)} &= h(x^{(t+1)}). \end{aligned} \quad (3)$$

The solution of system (3) is denoted by  $x^{(t)}(\xi)$  at time step  $t$  with initial condition  $x^{(0)} = \xi \in \mathcal{X}$ . We define the error term as  $e^{(t+1)} = x^{(t+1)} - \hat{x}^{(t+1)}$ . Then,

$$\begin{aligned} e^{(t+1)} &= x^{(t+1)} - W_{xa}\sigma(W_{ay}y^{(t+1)} + W_{ax}\hat{x}^{(t)}) \\ &= f(x^{(t)}) - W_{xa}\sigma(W_{ay}h(f(x^{(t)}))) \\ &\quad + W_{ax}x^{(t)} - W_{ax}e^{(t)}. \end{aligned} \quad (4)$$

Obviously,  $e^{(t+1)}$  is a function of  $e^{(t)}$  and  $x^{(t)}$ , and we call it the error system, denoted as follows,

$$e^{(t+1)} := g(e^{(t)}, x^{(t)}), \quad (5)$$

where  $e^{(t)} \in \mathcal{E} \subseteq \mathbb{R}^n$ , and  $\mathcal{E}$  is the space for the error term. In a similar manner, we denote the solution to system (5) as  $e^{(t)}(\eta, x)$  with the initial condition  $e^{(0)} = \eta \in \mathcal{E}$ .

We introduce Lyapunov functions for the error dynamics, regarding  $x^{(t)}$  as the input in (5).

**Definition 2.1:** A continuous function  $\alpha : \mathbb{R}_{\geq 0} \rightarrow \mathbb{R}_{\geq 0}$  is a  $\mathcal{K}$ -function if it is strictly increasing and  $\alpha(0) = 0$ . It is a  $\mathcal{K}_{\infty}$ -function if it is a  $\mathcal{K}$ -function and  $\alpha(r) \rightarrow \infty$  as  $r \rightarrow \infty$ .

**Definition 2.2:** A continuous function  $\beta : \mathbb{R}_{\geq 0} \times \mathbb{R}_{\geq 0} \rightarrow \mathbb{R}_{\geq 0}$  is a  $\mathcal{KL}$ -function if, for each fixed  $t$ , the function  $\beta(\cdot, t)$  is a  $\mathcal{K}$ -function with respect to  $r$ , and for each fixed  $r$ , the function  $\beta(r, \cdot)$  is decreasing with respect to  $t$ , and  $\beta(r, t) \rightarrow 0$  as  $t \rightarrow \infty$ .

**Definition 2.3:** The origin of (3) is globally asymptotically stable if, for each  $\varepsilon > 0$ , there is a  $\delta = \delta(\varepsilon) > 0$  such that

$$\|\xi\| < \delta \implies \|x^{(t)}\| < \varepsilon, \forall t \geq 0, \text{ and } \lim_{t \rightarrow \infty} x^{(t)} = 0. \quad (6)$$

In addition, there exists a  $\mathcal{KL}$ -function  $\beta$  such that

$$\|x^{(t)}(\xi)\| \leq \beta(\|\xi\|, t) \quad \forall \xi \in \mathcal{X}, \forall t \in \mathbf{Z}_+. \quad (7)$$

**Definition 2.4:** [24] The discrete-time system (5) is input-to-state stable (ISS) if there exists a  $\mathcal{KL}$ -function  $\beta$  and a  $\mathcal{K}$ -function  $\gamma$ , such that for each  $t \in \mathbf{Z}_+$ , the following inequality holds,

$$|e^{(t)}(\eta, x)| \leq \beta(\|\eta\|, t) + \gamma(\|x\|), \quad (8)$$

for all  $\eta \in \mathcal{E}$  and for all  $x \in \mathcal{X}$ .

**Definition 2.5:** [24] A continuous function  $V : \mathbb{R}^n \rightarrow \mathbb{R}_{\geq 0}$  is called an ISS-Lyapunov function for the discrete-time system (5) if there exist  $\mathcal{K}_{\infty}$ -functions  $\alpha_1, \alpha_2, \alpha_3$ , and a  $\mathcal{K}$ -function  $\gamma$  such that

$$\alpha_1(\|e^{(t)}\|) \leq V(e^{(t)}) \leq \alpha_2(\|e^{(t)}\|), \quad \forall e^{(t)} \in \mathcal{E}, \quad (9)$$

and

$$\begin{aligned} V(g(e^{(t)}, x^{(t)})) - V(e^{(t)}) &\leq -\alpha_3(\|e^{(t)}\|) + \gamma(\|x^{(t)}\|) \\ &\quad \forall e^{(t)} \in \mathcal{E}, \forall x^{(t)} \in \mathcal{X}. \end{aligned} \quad (10)$$

**Theorem 2.6:** If the error system (5) with  $x^{(t)}$  as input is ISS and the origin of the discrete-time system (3) is globally asymptotically stable, then the origin of the cascade system (3) and (5) is globally asymptotically stable.

*Proof:* The solutions of (3) and (5) satisfy:

$$\|x^{(t)}(\xi)\| \leq \beta_1(\|\xi\|, t), \quad (11)$$

$$\|e^{(t)}(\eta, x)\| \leq \beta_2(\|\eta\|, t) + \gamma(\|x^{(t)}\|), \quad (12)$$

where  $\beta_1, \beta_2$  are  $\mathcal{KL}$ -functions. Thus,

$$\|e^{(t)}(\eta, x)\| \leq \beta_2(\|\eta\|, t) + \gamma(\beta_1(\|\xi\|, t)). \quad (13)$$

Let  $s^{(t)}$  denote the concatenation of the state  $x^{(t)}$  and the error state  $e^{(t)}$ , and  $\zeta$  denote the origin of this cascade system. We have  $\|x^{(t)}\| \leq \|s^{(t)}\|$  and  $\|e^{(t)}\| \leq \|s^{(t)}\|$ , and  $\|s^{(t)}\| \leq \|x^{(t)}\| + \|e^{(t)}\|$ . Defining  $\beta(\cdot, \cdot) = \beta_1(\cdot, \cdot) + \beta_2(\cdot, \cdot) + \gamma(\beta_1(\cdot, \cdot))$ , this yields

$$\|s^{(t)}(\zeta)\| \leq \beta(\|\zeta\|, t) \quad \forall t \in \mathbf{Z}_+. \quad (14)$$

It can be easily verified that  $\beta$  is a  $\mathcal{KL}$ -function, which completes the proof.  $\blacksquare$

Two different approaches were used for finding the Lyapunov function, depending on whether the system is linear or nonlinear.

### A. Linear systems

Consider a linear discrete-time system defined by, for matrices  $A$  and  $H$ ,

$$\begin{aligned} x^{(t+1)} &= Ax^{(t)}, \\ y^{(t+1)} &= Hx^{(t+1)}. \end{aligned} \quad (15)$$

By using the identity function as the activation function  $\sigma$  in (2), the error dynamics of the linear state estimator can be written as

$$\begin{aligned} e^{(t+1)} &= Ax^{(t)} - W_{xa}(W_{ay}y^{(t+1)} + W_{ax}\hat{x}^{(t)}) \\ &= Ax^{(t)} - W_{xa}(W_{ay}Hx^{(t+1)} + W_{ax}(x^{(t)} - e^{(t)})) \\ &= (A - W_{xa}W_{ay}HA - W_{xa}W_{ax})x^{(t)} + W_{xa}W_{ax}e^{(t)}. \end{aligned} \quad (16)$$

Defining  $\mathcal{A} = W_{xa}W_{ax}$  and  $\mathcal{B} = A - W_{xa}W_{ay}HA - W_{xa}W_{ax}$ , the error system is a linear system with  $x^{(t)}$  as the input:

$$e^{(t+1)} = \mathcal{A}e^{(t)} + \mathcal{B}x^{(t)}. \quad (17)$$

If this discrete-time system is ISS then there is a quadratic Lyapunov function

$$V(e) = e^T P e, \quad (18)$$

where  $P$  is a positive definite matrix obtained by solving

$$\mathcal{A}^T P \mathcal{A} - \mathcal{A} + Q = 0. \quad (19)$$

Here,  $Q$  is a symmetric positive definite matrix. In this case, it is easy to show that both properties in Def. 2.5 are satisfied with  $\alpha_1(x) = \lambda_{\min}(P)x^2$ ,  $\alpha_2(x) = \lambda_{\max}(P)x^2$ ,  $\alpha_3(x) = \frac{1}{2}\lambda_{\min}(Q)x^2$ , and  $\gamma(x) = (\frac{2|\mathcal{A}^T P \mathcal{B}|^2}{\lambda_{\min}(Q)} + |\mathcal{B}^T P \mathcal{B}|^2)x^2$  [24].

### B. Nonlinear systems

For nonlinear systems, a counterexample-guided method with verification provided by SMT solvers was used to synthesize the ISS-Lyapunov functions for the error system (5).

Inspired by [25], we use a one-hidden layer feed-forward neural network with zero bias terms for all layers to learn a Lyapunov function of the following form

$$V(e; \theta) = \sigma(W_2 \sigma(W_1 e)), \quad (20)$$

where  $W_1$  and  $W_2$  are the weights for the hidden layer and output layer respectively,  $\theta$  denotes all the hyper-parameters,  $\sigma$  is the activation function,  $e$  is the input vector, which is the shorthand notation for the error state at time  $t$ . Similarly,  $x$  denotes the state at time  $t$ .

We use the square function as the activation function  $\sigma$  in this network, which results in sum-of-squares (SOS)-like quadratic Lyapunov functions. Consequently, we have  $V(0) = 0$ . As a result, a valid ISS Lyapunov function is attained when properties (9) and (10) are satisfied. Its falsification constraints can then be written as a first-order logic formula over the real numbers. This yields

$$\begin{aligned} &\left( \sum_{i=1}^n e_i^2 \leq r_e \vee \sum_{i=1}^n x_i^2 \leq r_x \right) \wedge \\ &\left( (V(x) - \alpha_1(|e|) \leq 0) \vee (V(x) - \alpha_2(|e|) \geq 0) \vee \right. \\ &\left. (V(g(e, x)) - V(e) + \alpha_3(|e|) - \gamma(|x|) \geq 0) \right), \end{aligned} \quad (21)$$

where,  $r_e$  and  $r_x$  are the radii of the so-called valid region for the error state and the state respectively, on which we verify the condition using SMT solvers. When the SMT solver returns UNSAT, a valid ISS Lyapunov function is obtained. Otherwise, it produces counterexamples that can be added to the training dataset of the neural network for finding Lyapunov function candidates. It is worth mentioning that due to the nature of the SMT solvers, we typically need to exclude a small region around the origin when verifying the falsification constraints. Around the origin, the linearization of the nonlinear system dominates, and we can implement the method for the linearized model to provide stability guarantees as detailed in Section II-A. We refer the readers to [26] for a detailed rigorous proof and algorithm.

The loss function is consistent with the falsification constraints:

$$\begin{aligned} L(\theta) &= \frac{1}{MN} \sum_{j=1}^M \sum_{i=1}^N \max \left( 0, V_\theta(g(e_i, x_j)) - V_\theta(e_i) \right. \\ &\quad \left. + \alpha_3(|e_i|) - \gamma(|x_j|) \right) + \max \left( 0, V_\theta(e_i) - \alpha_2(|e_i|) \right) \\ &\quad + \max \left( 0, \alpha_1(|e_i|) - V_\theta(e_i) \right). \end{aligned} \quad (22)$$

This is known as the positive penalty for the violation of conditions in Definition 2.5.

## III. IMPLEMENTATION

The initial conditions are sampled over an interval. The initial condition is considered to be Gaussian. The covariance of the initial condition is  $(0.01) \times I$  where  $I$  is an identity matrix of appropriate dimensions. Similarly, process and measurement noises are assumed to be Gaussian with zero mean and covariance  $0.01 \times I$  where matrix  $I$  is of appropriate dimensions. This is done for each sequence in the data set. Since the approach is state estimation, knowledge of the functions  $f$  and  $h$  in (1) is used in data generation.

The data set is divided into three parts: training, validation and testing in the ratio 80 : 10 : 10.

### A. Training and validation

A custom network with forward propagation as in (2) is implemented. The weight matrix  $W_{ay}$  is initialized using Xavier uniform distribution while weight matrices  $W_{ya}$  and  $W_{xa}$  are initialized to be (semi) orthogonal matrices using *Pytorch's torch.nn.init* module. The function  $\sigma(z)$  is chosen to be equal to  $z$  for linear systems and is chosen to be  $\tanh(z)$  for nonlinear systems. The backward propagation

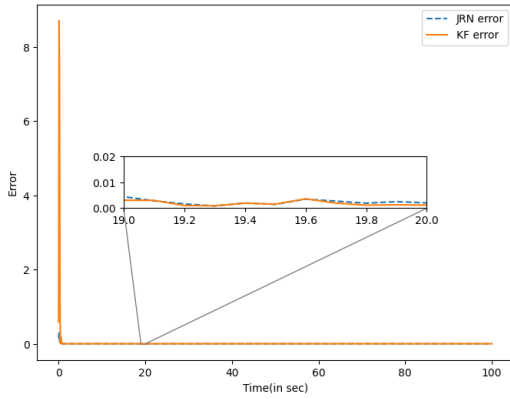


Fig. 2: The graph represents a comparison between JRN and KF Error( $t$ ),  $0 \leq t \leq 100$  values of Jordan recurrent network based state estimation and the Kalman filter based state estimation for mass-spring damper system. The magnified graph within the graph provides a closer look at the error values from time 19 to 20 seconds. The x-axis of both the original and the magnified graphs represents time in seconds while the y-axis represents error at time  $t$ . The blue dotted line graph represents the error values for JRN based estimates while the orange solid line represents the error values for the Kalman filter based estimates.

is implemented using *PyTorch*'s *backward()* function. The loss function at time-step  $t + 1$  for each sequence is

$$J_i^{(t+1)}(\phi) = \frac{1}{n} \sum_{i=1}^n (x_i^{(t+1)} - \hat{x}_{i,\phi}^{(t+1)})^2, \quad (23)$$

where  $1 \leq i \leq n$  and  $n$  is the number of states,  $x_i^{(t+1)}$  represents the true value of state  $x_i$  at time-step  $t + 1$  and  $\hat{x}_{i,\phi}^{(t+1)}$  represents the estimated value of state  $x_i$  at time-step  $t + 1$  by the JRN where  $\phi$  denotes hyper-parameters of the network. Adam optimization is used for training the network. The optimal learning rate is chosen based on the network's performance over a range of learning rates. The number of hidden units considered is 50 and a batch size of 40 is used for each example in Section IV.

Early stopping with a fixed patience value to decide the number of epochs needed is used. In each epoch, network's performance on validation data is used as the measure to decide whether to proceed or keep training for another epoch.

### B. Testing and comparison with KF and EKF

We tested our estimators for 3 different systems in Section IV by comparing the results with KF for the linear system and EKF for the nonlinear systems. Standard implementations of KF and EKF are used, see for example [2].

As mentioned earlier, 10% of the data set is used for testing. We compare JRN and EKF graphically using average error at time  $t$  over all features and all test sequences

$$\text{Error}(t) = \frac{1}{m_{test}n} \sum_{k=1}^{m_{test}} \sum_{i=1}^n (x_i^{(t)[k]} - \hat{x}_i^{(t)[k]})^2, \quad (24)$$

where  $m_{test}$  is the number of test sequences,  $n$  is the number of states,  $x_i^{(t)[k]}$  represents the true value of state  $x_i$  at time-step  $t$  for the  $k^{th}$  sequence and  $\hat{x}_i^{(t)[k]}$  represents the estimated value of state  $x_i$  at time-step  $t$  for the  $k^{th}$  sequence. We also use normalised mean square error (NMSE) to compare different methods. It is calculated as

$$\text{NMSE} = \frac{1}{m_{test}nT} \sum_{k=1}^{m_{test}} \sum_{j=1}^T \sum_{i=1}^n (x_i^{(j)[k]} - \hat{x}_i^{(j)[k]})^2, \quad (25)$$

where  $m_{test}$  is the number of test sequences,  $T$  is the number of time-steps in each sequence,  $n$  is the number of states,  $x_i^{(j)[k]}$  represents the true value of state  $x_i$  at time-step  $j$  for the  $k^{th}$  sequence and  $\hat{x}_i^{(j)[k]}$  represents the estimated value of state  $x_i$  at time-step  $j$  for the  $k^{th}$  sequence.

## IV. NUMERICAL RESULTS

In this section, we illustrate the proposed method with several examples. All three discrete-time systems were obtained by discretizing common ordinary differential equation examples. We use a zero order hold discretization for linear systems. For nonlinear continuous-time state space systems, we use the RK-45 discretization using Python's *scipy.integrate.solve\_ivp* function.

A remote Windows server with T4 GPU, courtesy of math faculty computing facility (MFCF), University of Waterloo, was used for all numerical simulations.

### A. Mass-Spring-Damper system

Consider a zero order hold discretization with  $\Delta t = 0.1s$  of the mass-spring damper system

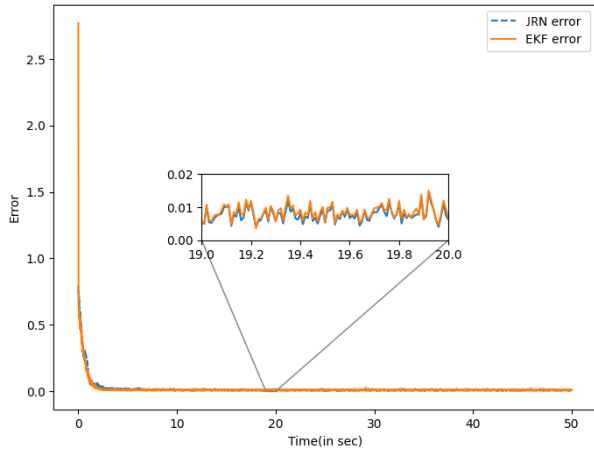
$$\dot{\mathbf{x}}(t) = \begin{bmatrix} \dot{x}_1(t) \\ \dot{x}_2(t) \end{bmatrix} = \begin{bmatrix} x_2(t) \\ -\frac{k}{m}x_1(t) - \frac{b}{m}x_2(t) \end{bmatrix}, \quad (26)$$

where  $x_1(t)$  and  $x_2(t)$  are the position and velocity respectively of the spring. The parameters are  $m = 10kg$ ,  $b = 6kg/sec$  and  $k = 800kg/sec^2$ . The measurement vector at time-step  $t$  is  $y^{(t)} = x_1^{(t)} + \nu^{(t)}$  where  $\nu^{(t)}$  is the measurement noise at time-step  $t$ .

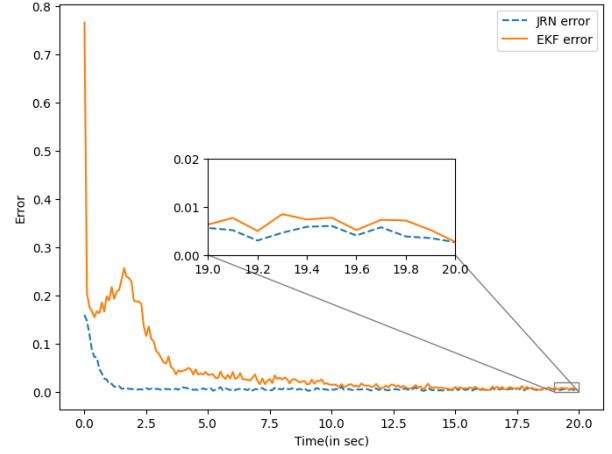
We consider 100 sequences from 0 to 100 seconds each. The mean of the initial condition is chosen randomly from  $[-1, 1] \times [-1, 1]$ . Early stopping was implemented with a patience of 5. We use Adam optimization for training with a learning rate of  $10^{-4}$ . There were 4216 epochs for training.

Fig. 2 shows the error at each time-step averaged all test sequences for JRN and EKF. As can be seen from Fig. 2, the error for JRN converges to 0 as fast as for the KF. Also, the NMSE for JRN is 0.0631 and for KF is 0.0653 which is very close. Recall that KF is the optimal estimator for this system. Since the initial condition is not assumed to be known by the estimator, there is a spike in the initial values of the error for the KF and the JRN but the spike in KF error is considerably larger than that of JRN. The magnified graph in Fig. 2 shows that after convergence JRN error is very close to that the KF error.

For this 2-dimensional linear system, the origin is asymptotically stable. We then implement the method in II-A for



(a) Comparison between JRN and EKF Error( $t$ ) values for time  $0 \leq t \leq 50$  seconds for down pendulum.



(b) Comparison between JRN and EKF Error( $t$ ) values for time  $0 \leq t \leq 20$  seconds for reversed Van der Pol oscillator.

Fig. 3: The graphs represent a comparison of Error( $t$ ) values of Jordan recurrent network-based state estimation and extended Kalman filter-based state estimation for nonlinear dynamical systems. The magnified graph within each graph provides a closer look at the error values from time 19 to 20 seconds. The x-axis of both the original and the magnified graphs represents time in seconds, while the y-axis represents error at time  $t$ . The blue dotted line graph represents the error values for JRN-based estimates, while the orange solid line represents the error values for extended Kalman filter-based estimates.

linear systems. Setting  $Q = I$ , it is easy to establish that  $P = \begin{bmatrix} 1.0236 & -0.0934 \\ -0.0934 & 69.4428 \end{bmatrix}$ . With this ISS-Lyapunov function, by Theorem 2.6, both the original system and the error system are asymptotically stable. This proves the stability of the NN estimator error.

### B. Down pendulum

Consider an RK-45 discretization with  $\Delta t = 0.01s$  of the down pendulum

$$\dot{\mathbf{x}}(t) = \begin{bmatrix} \dot{x}_1(t) \\ \dot{x}_2(t) \end{bmatrix} = \begin{bmatrix} x_2(t) \\ -\frac{g}{l} \sin(x_1(t)) - \frac{b}{m} x_2(t) \end{bmatrix}, \quad (27)$$

where  $x_1(t)$  and  $x_2(t)$  are the position and velocity of the pendulum respectively. The parameters are  $g = 9.8m/sec^2$ ,  $m = 2kg$ ,  $b = 0.9kg/sec$  and  $l = 1m$ . The measurement vector at time-step  $t$  is  $y^{(t)} = x_1^{(t)} + \nu^{(t)}$  where  $\nu^{(t)}$  is the measurement noise at time-step  $t$ .

We consider 200 sequences from 0 to 50 seconds each. The mean of the initial condition is chosen randomly from  $[-2, 2] \times [-2, 2]$ . Early stopping was implemented with a patience of 50. The validation loss reached early stopping patience at 2984 epochs. We further used Adam optimization for training with a learning rate of  $10^{-4}$ .

The error at each time-step, averaged over all features and all test sequences, is shown for JRN and EKF in Fig. 3a. The

error for JRN converges to 0 as fast as that for the EKF. Also, the NMSE for JRN is 0.0627 while for EKF it is 0.0647. The magnified graph in Fig. 3a shows that after convergence JRN error and EKF error are quite close. The initial spike in JRN error is not as high as the EKF error. The error becomes very small as  $t$  goes to  $\infty$ , despite the presence of noise.

For this nonlinear system, an ISS Lyapunov function was learned using a neural network, as shown in Fig. 4, which is verified by an SMT solver, dReal [27], on a  $[-4, 4]$  for the error state. In this case, we used  $\alpha_1(\cdot) = \alpha_3(\cdot) = 0.01|\cdot|$  and  $\alpha_2(\cdot) = \gamma(\cdot) = 100|\cdot|$ .

### C. Reversed Van der Pol oscillator

Consider an RK-45 discretization with  $\Delta t = 0.1s$  of the reversed Van der Pol oscillator

$$\dot{\mathbf{x}}(t) = \begin{bmatrix} \dot{x}_1(t) \\ \dot{x}_2(t) \end{bmatrix} = \begin{bmatrix} -x_2(t) \\ x_1(t) + ((x_1(t))^2 - 1)x_2(t) \end{bmatrix} \quad (28)$$

where  $x_1(t)$  and  $x_2(t)$  is the position and velocity of the oscillator. The measurement vector at time-step  $t$  is  $y^{(t)} = x_1^{(t)} + \nu^{(t)}$  where  $\nu^{(t)}$  is the measurement noise at time-step  $t$ .

We consider 200 sequences from 0 to 20 seconds each. The mean of the initial condition is chosen randomly from  $[-1, 1] \times [-1, 1]$ . The training was done for 35000 epochs as early stopping patience of 7000 was not achieved. The



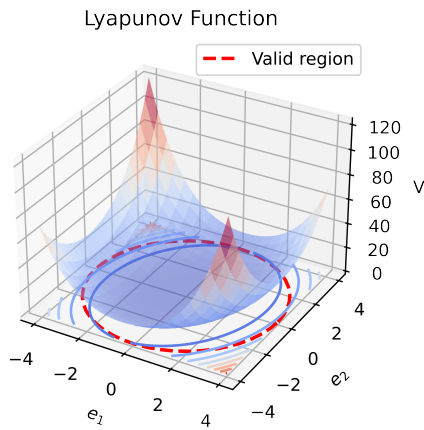


Fig. 4: The learned ISS Lyapunov function for the down pendulum example.

validation error continued to decrease. Adam optimization is used for training with a learning rate of  $10^{-4}$ . As can be seen from Fig. 3b, the JRN error converges to zero much faster than the EKF error. Also, the NMSE for JRN is 0.0484 while for EKF is 0.1025. This is considerable difference. The magnified graph shows that even after convergence, the JRN error is better than EKF error. This example suggests that when a network is trained for a larger number of epochs, the JRN error can converge much faster than the EKF error.

For this system, in a similar manner to the previous example, we synthesized an ISS-Lyapunov function on  $[-2, 2]$  for the error states, which provides the asymptotic stability for the error term by Theorem 2.6.

## V. CONCLUSIONS AND FUTURE WORK

In this paper, we demonstrated that when knowledge of functions  $f$  and  $h$  in (1) is available or the data of the real systems can be properly sampled, state estimation can be performed by using Jordan recurrent networks. The Jordan recurrent network based estimator helped us achieve results as good as KF and EKF. We also showed the stability of the error dynamics of the neural estimator using an ISS approach, by taking advantage of the structural properties of an unbiased JRN. For linear systems, quadratic Lyapunov equations can be computed analytically for the error dynamics to provide stability. For nonlinear systems, a counter-example guided method was used to learn an ISS Lyapunov function. Furthermore, the effectiveness of the proposed method has been illustrated with three 2-dimensional systems. We will extend our approach to higher dimensional systems in future research. Another potential future research direction is to consider stability for the case where biases are non-zero.

Additional further work is to extend the results on the convergence of discrete-time recurrent neural networks as shown in [28] to JRN.

## REFERENCES

- [1] R. E. Kalman, "A new approach to linear filtering and prediction problems." *J. Basic Eng.*, vol. 82, no. 1, pp. 35–45, 1960.
- [2] D. Simon, *Optimal State Estimation: Kalman,  $H^\infty$ , and Nonlinear Approaches*. Wiley-Interscience, 2006.
- [3] K. A. Morris, *Introduction to Feedback Control*. Harcourt/Academic Press, 2001.
- [4] A. J. Krener, "The convergence of the extended kalman filter," *Directions in Mathematical Systems Theory and Optimization (Lecture Notes in Control and Information Sciences)* by Rantzer and Byrnes, Eds. Berlin, Germany, vol. 286, pp. 173–182, 2003.
- [5] S. Afshar, F. Germ, and K. Morris, "Extended kalman filter based observer design for semilinear infinite-dimensional systems," *IEEE Transactions on Automatic Control*, 2023.
- [6] C. Gao, J. Yan, S. Zhou, P. K. Varshney, and H. Liu, "Long short-term memory-based deep recurrent neural networks for target tracking," *Information Sciences*, vol. 502, pp. 279–296, 2019.
- [7] R. Deep, *Probability and statistics: with integrated software routines*. Academic Press, 2006.
- [8] T. Breiten and K. Kunisch, "Neural network based nonlinear observers," *Systems & Control Letters*, vol. 148, p. 104829, 2021.
- [9] J. Peralez and M. Nadri, "Deep learning-based luenberger observer design for discrete-time nonlinear systems," *60th IEEE Conference on Design and Control*, pp. 4370–4375, 2021.
- [10] R. Gencay and T. Liu, "Nonlinear modelling and prediction with feedforward and recurrent networks," *Physica D: Nonlinear Phenomena*, vol. 108, no. 1-2, pp. 119–134, 1997.
- [11] J. Park, D. Yi, and S. Ji, "Analysis of recurrent neural network and predictions," *Symmetry*, vol. 12, no. 4, p. 615, 2020.
- [12] Z. Kasiran, Z. Ibrahim, and M. S. M. Ribuan, "Mobile phone customers churn prediction using elman and jordan recurrent neural network," *7th international conference on computing and convergence technology (ICCCCT)*, pp. 673–678, 2012.
- [13] W. Wu, S.-Y. An, P. Guan, D.-S. Huang, and B.-S. Zhou, "Time series analysis of human brucellosis in mainland china by using elman and jordan recurrent neural networks," *BMC infectious diseases*, vol. 19, pp. 1–11, 2019.
- [14] C.-M. Kuan, K. Hornik, and H. White, "A Convergence Result for Learning in Recurrent Neural Networks," *Neural Computation*, vol. 6, no. 3, pp. 420–440, 1994.
- [15] J. P. Llerena Cana, J. Garcia Herrero, and J. M. Molina Lopez, "Forecasting nonlinear systems with lstm: analysis and comparison with ekf," *Sensors*, vol. 21, no. 5, p. 1805, 2021.
- [16] E. Kandiran and A. Hacinliyan, "Comparison of feedforward and recurrent neural network in forecasting chaotic dynamical system," *AJIT-e: Academic Journal of Information Technology*, vol. 10, no. 37, pp. 31–44, 2019.
- [17] I. Goodfellow, Y. Bengio, and A. Courville, *Deep Learning*. The MIT Press, Cambridge, Massachusetts, 2016.
- [18] A. M. Schäfer and H.-G. Zimmermann, "Recurrent neural networks are universal approximators," *International journal of neural systems*, vol. 17, no. 04, pp. 253–263, 2007.
- [19] A. Kaur and K. A. Morris, "State estimator design using jordan based long short-term memory networks." preprint, 2024.
- [20] N. E. Barabanov and D. V. Prokhorov, "Stability analysis of discrete-time recurrent neural networks," *IEEE Transactions on Neural Networks*, vol. 13, no. 2, pp. 292–303, 2002.
- [21] J. N. Knight, *Stability analysis of recurrent neural networks with applications*. Colorado State University, 2008.
- [22] Y.-C. Chang, N. Roohi, and S. Gao, "Neural lyapunov control," *Advances in neural information processing systems*, vol. 32, 2019.

- [23] R. Zhou, T. Quartz, H. De Sterck, and J. Liu, "Neural lyapunov control of unknown nonlinear systems with stability guarantees," *Advances in Neural Information Processing Systems*, vol. 35, pp. 29113–29125, 2022.
- [24] Z.-P. Jiang and Y. Wang, "Input-to-state stability for discrete-time nonlinear systems," *Automatica*, vol. 37, no. 6, pp. 857–869, 2001.
- [25] A. Abate, D. Ahmed, A. Edwards, M. Giacobbe, and A. Peruffo, "Fossil: a software tool for the formal synthesis of lyapunov functions and barrier certificates using neural networks," in *Proceedings of the 24th International Conference on Hybrid Systems: Computation and Control*, pp. 1–11, 2021.
- [26] J. Liu, Y. Meng, M. Fitzsimmons, and R. Zhou, "Physics-informed neural network lyapunov functions: Pde characterization, learning, and verification," *arXiv preprint arXiv:2312.09131*, 2023.
- [27] S. Gao, S. Kong, and E. M. Clarke, "dreal: An smt solver for nonlinear theories over the reals," in *International conference on automated deduction*, pp. 208–214, Springer, 2013.
- [28] Z. Yi, *Convergence analysis of recurrent neural networks*, vol. 13. Springer Science & Business Media, 2013.